

Macroparasite dynamics of migratory host populations

Stephanie J. Peacock^{a,b,c,*}, Juliette Bouhours^d, Mark A. Lewis^{b,d}, Péter K. Molnár^{a,e}

^a*Ecology and Evolutionary Biology, University of Toronto*

^b*Biological Sciences, University of Alberta*

^c*Current address: Biological Sciences, University of Calgary*

^d*Mathematical and Statistical Sciences, University of Alberta*

^e*Biological Sciences, University of Toronto Scarborough*

Abstract

Spatial variability in host density is a key factor affecting disease dynamics of wildlife, and yet there are few spatially explicit models of host-macroparasite dynamics. This limits our understanding of parasitism in migratory hosts, whose densities change considerably in both space and time. In this paper, we develop a model for host-macroparasite dynamics that considers the directional movement of host populations and their associated parasites. We include spatiotemporal changes in the mean and variance in parasite burden per host, as well as parasite-mediated host mortality and parasite-mediated migratory ability. Reduced migratory ability with increasing parasitism results in heavily infested hosts halting their migration, and higher parasite burdens in stationary hosts than in moving hosts. Simulations reveal the potential for positive feedbacks between parasite-reduced migratory ability and increasing parasite burdens at infection hotspots, such as stopover sites, that may lead to parasite-induced migratory stalling. This framework may be useful for future exploration of how global change might influence wildlife disease via changes to migratory patterns and parasite demographic rates.

Keywords: macroparasite; population; animal migration; disease; partial-differential equation; spatial dynamics

1. Introduction

Many animals undergo arduous migrations to track season changes in environmental conditions and resources, and the resulting spatiotemporal changes in host density have implications for parasite dynamics (Altizer et al., 2011). For example, host migration may facilitate the spread of parasites into new areas where they might infect novel host species. This is of increasing concern in the face of climate change, when warming temperatures are allowing parasites to persist where they previously could not (e.g., Kutz et al., 2013).

*stephanie.j.peacock@gmail.com

8 Alternately, migratory hosts may escape parasitism by moving away from infection hotspots
9 where parasites have accumulated in the environment (Bartel et al., 2011). For example,
10 migratory escape has been proposed as a driver of post-calving migration in caribou (Folstad
11 et al., 1991). Migratory lifecycles may also reduce transmission of parasites from adults to
12 juveniles, termed migratory allopatry, as is the case for sea louse parasites of Pacific salmon
13 (Krkošek et al., 2007). Mechanisms such as parasite spread and migratory escape may
14 interact and depend on the life histories of both parasites and hosts, making it difficult
15 to understand the net impact of migration on host-parasite dynamics. Further, changes
16 in host-parasite dynamics due to, for example, climate change (Kutz et al., 2013) or the
17 introduction of reservoir hosts (Krkošek et al., 2007; Morgan et al., 2007) may change how
18 migration influences host-parasite dynamics.

19 Mathematical models describing the growth and spread of infectious pathogens through
20 a host population have been integral to the understanding of disease dynamics in both
21 human and wildlife populations (May and Anderson, 1991; Hudson et al., 2002). Two basic
22 structures have been applied in modelling disease dynamics. Compartmental models track
23 the transition of hosts between susceptible (S) and infected (I) categories and thus describe
24 the prevalence of infection within the host population. Sometimes immune or recovered (R)
25 hosts are also considered, leading to the common designation as SIR models. These models
26 are typically used to describe microparasites (e.g., viruses, bacteria) where the impact of the
27 parasite is assumed to be independent of the number of parasites infecting a host (Anderson
28 and May, 1979).

29 Several recent studies have used SIR-type models to understand and predict parasite
30 dynamics in migratory wildlife (e.g., Hall et al., 2014; Johns and Shaw, 2015; Hall et al.,
31 2016). These models tracked the densities of susceptible and infected hosts at different
32 stages in the annual cycle (e.g., breeding, migration, and overwintering). Hall et al. (2014)
33 describe an SI model in which mortality of host populations during migration depends on
34 their parasite burden at the end of the breeding or overwintering season. They found that

35 migration lowers pathogen prevalence via culling of infected hosts, and thus host population
36 health improved with earlier departure and longer-distance migrations. Johns and Shaw
37 (2015) built upon that model to look at disease prevalence in migratory vs. non-migratory
38 populations with similar results: host populations ended up healthier if they spent more
39 time migrating and had higher mortality during migration due to disease or other factors.
40 More recent work has also considered vector-borne diseases and how changing phenology
41 with climate change might lead to “migratory mismatch” of host and vector densities (Hall
42 et al., 2016).

43 Macroparasite dynamics require a different model structure because their impact on
44 hosts is often proportional to parasite burden, as is typical for many helminths (parasitic
45 worms; e.g., tapeworms, flukes) or ectoparasites (e.g., ticks, lice). Macroparasites also tend
46 to be aggregated among hosts (Shaw et al., 1998). Explicitly considering the intensity of
47 infection and the degree of aggregation is important in macroparasite models because the
48 mortality of heavily infected hosts will result in disproportionate mortality in the parasite
49 population (Anderson and May, 1978). A less-recognized complication is that the degree of
50 aggregation will change with any process that tends to select heavily infested hosts, such as
51 parasite-induced host mortality, with subsequent impacts on parasite population dynamics.
52 This additional complexity has hindered the development of spatially explicit models for
53 macroparasite dynamics (Riley et al., 2015). Spatial effects have been *implicitly* included in
54 macroparasite models via spatial patchiness in infection pressure (Cornell et al., 2004; May,
55 1978) or discrete geographic areas (Morgan et al., 2007), but models that *explicitly* track the
56 movement of hosts and their parasites have been lacking (but see Milner and Zhao, 2008,
57 who consider passive flow of parasites in a river system).

58 Explicitly spatial macroparasite models are needed to understand and predict how host
59 movement and parasitism might interact to affect wildlife health, which is especially im-
60 portant for migratory species. Existing models of parasite dynamics in migratory animals
61 (e.g., Hall et al., 2014; Johns and Shaw, 2015; Hall et al., 2016; Morgan et al., 2007) do not

62 consider how parasite burdens change dynamically over time and space or incorporate the
63 dynamic processes occurring during movement that might influence parasite burdens, such
64 as transmission and parasite-mediated migratory ability. These shortcomings not only limit
65 our understanding for macroparasites, but ignore important aspects of host biology. Ani-
66 mals with high parasite burdens often show reduced migratory ability (Risely et al., 2017).
67 For example, monarch butterflies infested with protozoan parasites are slower and fly shorter
68 distances (Bradley and Altizer, 2005) and juvenile salmon infested with sea lice have reduced
69 swimming performance (Nendick et al., 2011) and compromised schooling behavior (Krkošek
70 et al., 2011). Parasite-mediated migratory ability may affect both the spatial distribution of
71 hosts, limiting those that are able to complete their migration, and the spatial patterns in
72 parasite burden, resulting in higher parasite burdens of stationary hosts left behind.

73 Here, we develop a new modelling framework for migratory-host and macroparasite pop-
74 ulation dynamics that considers dynamic changes in host abundance, parasite burden, and
75 parasite aggregation. This extends previous host-macroparasite models (e.g., Anderson and
76 May, 1978; Kretzschmar and Adler, 1993) to explicitly include spatial representation of a
77 migration corridor. Parasite aggregation, as well as abundance, is allowed to change dynam-
78 ically in space and time as a consequence of multiple interacting demographic, spatial, and
79 epidemiological processes. First, we introduce the model and then we explore the model-
80 predicted dynamics under a range of parameters. These simulation exercises provide new
81 insights, such as the potential for parasite-mediated migratory stalling, and hint at the po-
82 tential for broader application of the model in future studies.

83 **2. Model**

84 We develop a model that tracks changes in host abundance, parasite burden, and the
85 aggregation of parasites along a one-dimensional migration corridor using a system of partial
86 differential equations (PDEs). The model includes potential impacts of parasite burden on
87 the migratory ability of hosts by dividing the host population into two categories: those

Table 1: Abundance variables* in the migratory host-macroparasite model.

Symbol	Description
p_i	Abundance of stationary hosts with i parasites at (x, t)
$N = \sum_{i=0}^{\infty} p_i$	Abundance of the total stationary host population at (x, t)
$P = \sum_{i=0}^{\infty} ip_i$	Abundance of the total parasites on stationary hosts at (x, t)
$r_i = p_i/N$	Proportion of stationary hosts with i parasites
$m = P/N$	Mean parasite burden of stationary hosts
A	Variance-to-mean ratio (VMR) of parasites on stationary hosts
L	Density of infectious parasite larvae in the environment (section 2.2)

*Variables are all dependent on space and time (i.e., $p_i = p_i(x, t)$) but we have dropped the (x, t) for brevity. The variable for stationary hosts is shown, but the same variable exists for moving hosts, denoted by $\hat{\cdot}$.

88 that are moving at a constant speed and those that are stationary. We consider the rate
 89 at which hosts change from moving to stationary (i.e., stopping) or stationary to moving
 90 (i.e., starting) to be a function of parasite burden. We also consider how the aggregation
 91 of parasites in the host population might change as the host population migrates (Adler
 92 and Kretzschmar, 1992; Kretzschmar and Adler, 1993). In the following section, we develop
 93 equations describing the spatiotemporal changes in host abundance, mean parasite burden,
 94 and the variance-to-mean ratio in the parasite distribution among hosts.

95 *2.1. Birth, death, stopping, and starting*

96 Following the approach of Anderson and May (1978) and Kretzschmar and Adler (1993),
 97 we begin with a system of differential equations that describe the number of hosts with i
 98 parasites, p_i . We extend the model of Kretzschmar and Adler (1993) to include a spatial
 99 component, and distinguish moving and stationary hosts, where $p_i(x, t)$ is the number of
 100 stationary hosts with i parasites at location x and time t , and $\hat{p}_i(x, t)$ is the number of
 101 moving hosts at location x and time t . For all variables, we use $\hat{\cdot}$ to denote the moving
 102 population. Moving hosts stop at parasite-dependent rate γ_i and stationary hosts start
 103 moving at parasite-dependent rate ω_i . Other parameters in the model do not directly depend

104 on whether hosts are moving or stationary. Hosts are born parasite-free and stationary at
105 rate β ; we assume the host birth is independent of parasite burden, although this assumption
106 could be relaxed in future models (e.g., Dobson and Hudson, 1992). Hosts die at natural
107 rate μ , with additive parasite-induced mortality at per-parasite rate α . Parasites attach at
108 rate ϕ (see section 2.2), reproduce within the host at rate ρ , and die at rate σ . We assume
109 that parasite demographic rates are density independent, except that the rate of parasite-
110 induced host death depends on parasite burden. The basic model is described by four partial
111 differential equations:

$$\frac{\partial p_0}{\partial t} = \beta \sum_{i=0}^{\infty} (p_i + \hat{p}_i) - (\mu + \phi)p_0 + \sigma p_1 + \gamma_0 \hat{p}_0 - \omega_0 p_0 \quad (1)$$

$$\frac{\partial p_i}{\partial t} = -(\mu + \phi + i(\alpha + \sigma + \rho))p_i + \sigma(i+1)p_{i+1} + \phi p_{i-1} + \rho(i-1)p_{i-1} + \gamma_i \hat{p}_i - \omega_i p_i \quad (2)$$

$$\frac{\partial \hat{p}_0}{\partial t} - c \frac{\partial \hat{p}_0}{\partial x} = -(\mu + \phi)\hat{p}_0 + \sigma \hat{p}_1 - \gamma_0 \hat{p}_0 + \omega_0 p_0 \quad (3)$$

$$\frac{\partial \hat{p}_i}{\partial t} - c \frac{\partial \hat{p}_i}{\partial x} = -(\mu + \phi + i(\alpha + \sigma + \rho))\hat{p}_i + \sigma(i+1)\hat{p}_{i+1} + \phi \hat{p}_{i-1} + \rho(i-1)\hat{p}_{i-1} - \gamma_i \hat{p}_i + \omega_i p_i \quad (4)$$

112 Descriptions of the variables and parameters are given in Tables 1 and 2, respectively.
113 In Appendix A, we show that the solution to equations (1-4) and equation (5) are bounded,
114 positive, and unique for all $t \geq 0$, $x \in \Omega$, and $i \in \{0, \dots, I\}$, where I is some number of
115 parasites larger than the carrying capacity of hosts, provided $p_i(0, x)$, $\hat{p}_i(0, x)$, and $L(0, x)$
116 are non-negative, continuously differentiable, and integral in \mathbb{R} .

117 2.2. Attachment rate

118 The per-host attachment of parasites takes place at rate ϕ , in proportion to the number
119 of infectious parasites at (x, t) . We derive a formula for ϕ by considering a transmission stage
120 of larval parasites, $L(x, t)$, that are free-living, such as eggs, spores, or cysts. These larval

Table 2: Parameters in the migratory host-macroparasite model.

Symbol	Description	Baseline value	Units
β	Host birth	0	yr ⁻¹
μ	Natural host mortality	0	yr ⁻¹
ϕ	Parasite attachment	see section 2.2	yr ⁻¹
α	Parasite-induced host mortality	0.1	parasite ⁻¹ yr ⁻¹
ρ	Within-host parasite reproduction	0	parasite ⁻¹ yr ⁻¹
σ	Within-host parasite mortality	5	parasite ⁻¹ yr ⁻¹
κ	Production of free-living parasites	1	yr ⁻¹
λ	Infection probability	0.01	
μ_L	Mortality of free-living parasites	5	yr ⁻¹
c	Migration speed	10 000	km yr ⁻¹
γ	Stopping rate	1	yr ⁻¹
θ	Per-parasite increase in stopping	0	parasite ⁻¹ yr ⁻¹
ω	Starting rate	1	yr ⁻¹

121 parasites exist outside of the (primary) host and are assumed to be stationary relative to
 122 the distances moved by the migratory host population. The dynamics of the larval parasites
 123 are described by:

$$\frac{\partial L}{\partial t} = \kappa(P + \hat{P}) - \mu_L L - \lambda L(N + \hat{N}), \quad (5)$$

124 where κ is the within-host rate of production of larvae by attached parasites, P and \hat{P} are
 125 the total densities of attached parasites on stationary and moving hosts, respectively, μ_L is
 126 the mortality rate of larval parasites, λ is the infection probability, and N and \hat{N} are the
 127 densities of stationary and moving hosts, respectively (see section 2.4). The per-host rate of
 128 attachment is therefore $\phi = \lambda L$.

129 In cases where the development time of eggs, cysts, or spores is short, it may be justifiable
 130 to assume that the dynamics of parasite production and attachment occur on much faster
 131 timescales than the lifespans of hosts and parasites (Anderson and May, 1978). We refer to
 132 this as direct transmission because the time that parasite larvae spend in the environment
 133 is assumed to be negligible. In the case of direct transmission, we can assume that equation

134 (5) is at equilibrium or quasi-equilibrium:

$$L^* = \frac{\kappa(P + \hat{P})}{\mu_L + \lambda(N + \hat{N})}, \quad (6)$$

135 in which case the attachment rate becomes:

$$\phi = \lambda L^* = \frac{\kappa(P + \hat{P})}{\mu_L/\lambda + N + \hat{N}}. \quad (7)$$

136 The timescale assumption eliminates the need to track the dynamics of L explicitly. However,
137 we have chosen to model L explicitly as the balance between larval development and mortality
138 rates and host movement are a key factors controlling infection rates for migratory hosts and
139 allowing for dynamics like migratory escape.

140 2.3. Movement status

141 Hosts are classified as either stationary or moving. Moving hosts migrate at a constant
142 speed, c , regardless of the number of parasites they harbour, but hosts stop moving at
143 parasite-dependent rate γ_i and stationary hosts start moving at parasite-dependent rate ω_i .
144 We assume that the stopping rate increases linearly with the number of parasites in or on
145 a host: $\gamma_i = \gamma + \theta i$, where θ is the per-parasite increase in the stopping rate. Although
146 a saturating stopping rate may be more realistic, once γ_i becomes much greater than ω_i ,
147 most hosts will be stationary and the rate of stopping becomes biologically irrelevant. We
148 assume for our analysis that the rate of starting does not, however, depend on parasites
149 and thus all $\omega_i = \omega$, although this assumption could be relaxed depending on the system of
150 interest. For an initial exploration of the model's behavior, this seems to be a biologically
151 reasonable assumption because if an individual's ability to migrate is adversely affected by
152 parasites, they may still experience the drive to complete the migration, but as parasite
153 burden increases their progress will be hindered as they make increasingly frequent stops.

154 *2.4. Equations for the total population size*

155 We can write equations for the total host population (N and \hat{N}) and total parasite
 156 population (P and \hat{P}) at (x, t) by summing equations for p_i and \hat{p}_i over all possible numbers
 157 of parasites (Table 1). The aggregate equations are:

$$\frac{\partial N}{\partial t} = \beta(N + \hat{N}) - (\mu + \omega)N - \alpha P + \gamma \hat{N} + \theta \hat{P} \quad (8)$$

$$\frac{\partial P}{\partial t} = \rho P - (\mu + \omega + \sigma)P + \phi N + \gamma \hat{P} - \alpha N \sum_{i=0}^{\infty} i^2 r_i + \theta \hat{N} \sum_{i=0}^{\infty} i^2 \hat{r}_i \quad (9)$$

$$\frac{\partial \hat{N}}{\partial t} - c \frac{\partial \hat{N}}{\partial x} = -(\mu + \gamma) \hat{N} - (\alpha + \theta) \hat{P} + \omega N \quad (10)$$

$$\frac{\partial \hat{P}}{\partial t} - c \frac{\partial \hat{P}}{\partial x} = \rho \hat{P} - (\mu + \sigma + \gamma) \hat{P} + \phi \hat{N} + \omega P - \hat{N}(\alpha + \theta) \sum_{i=0}^{\infty} i^2 \hat{r}_i, \quad (11)$$

158 where r_i and \hat{r}_i are the proportion of stationary and moving hosts, respectively, harbouring i
 159 parasites (Table 2). The original model in equations (1-4) cannot be completely described by
 160 the above equations because the summations over r_i require information on the distribution
 161 of parasites among hosts.

162 *2.5. Mean parasite burden and the variance-to-mean ratio*

163 The mean parasite burden is the expected number of parasites that a host would have. To
 164 provide a more biologically intuitive measure of the infection level, we can rewrite equations
 165 (8-11) as a function of the mean parasite burdens per host, m and \hat{m} . The variables m and
 166 \hat{m} are well defined because N and \hat{N} remain positive for all t and x (Appendix A). Using
 167 the chain rule:

$$\frac{\partial m}{\partial t} = \frac{1}{N} \frac{\partial P}{\partial t} - \frac{m}{N} \frac{\partial N}{\partial t}. \quad (12)$$

168 We also introduce the variance-to-mean ratio (VMR), A , which describes the aggregation
 169 of parasites among hosts. We can write the summations in equations (8-11) in terms of the

170 VMR:

$$\sum_{i=0}^{\infty} i^2 r_i = \text{variance} + m^2 = m(A + m). \quad (13)$$

171 Calculating the change in mean number of parasites per host using equation (13) we arrive

172 at:

$$\frac{\partial N}{\partial t} = \beta(N + \hat{N}) - (\mu + \omega + \alpha m)N + (\gamma + \theta \hat{m})\hat{N} \quad (14)$$

$$\frac{\partial m}{\partial t} = \rho m + \phi - m \left(\sigma + \alpha A + \beta \left(\frac{N + \hat{N}}{N} \right) \right) + \frac{\hat{N}}{N} \left(\gamma(\hat{m} - m) + \theta \hat{m}(\hat{A} + \hat{m} - m) \right) \quad (15)$$

$$\frac{\partial \hat{N}}{\partial t} - c \frac{\partial \hat{N}}{\partial x} = -(\mu + \gamma + (\alpha + \theta)\hat{m})\hat{N} + \omega N \quad (16)$$

$$\frac{\partial \hat{m}}{\partial t} - c \frac{\partial \hat{m}}{\partial x} = \rho \hat{m} + \phi - \hat{m} \left(\sigma + (\alpha + \theta)\hat{A} \right) + \frac{N}{\hat{N}} \omega (m - \hat{m}). \quad (17)$$

173 As previously mentioned, macroparasites are often aggregated among hosts with a distri-
 174 bution that is well described by the negative binomial (Shaw et al., 1998). Thus, we proceed
 175 by assuming that parasites are distributed according to the negative binomial with mean
 176 parasite burden m and overdispersion parameter k . The VMR is related to the overdispersion
 177 parameter by $k = m/(A - 1)$. Although many macroparasite models assume that k is
 178 constant (and therefore the VMR changes predictably with the mean) (e.g., Anderson and
 179 May, 1978; May, 1978; Krkošek et al., 2011), we do not make this simplifying assumption
 180 because we expect that the aggregation of parasites among hosts will change in space and
 181 time with parasite-mediated migratory behaviour and parasite-induced host mortality. In
 182 the following section, we follow the approach of Kretzschmar and Adler (1993) and derive
 183 the equation for the VMR as an additional dynamic variable.

184 *2.6. Variance-to-mean ratio as a dynamic variable*

185 We derived equations for the change in the VMR of parasites on stationary and moving
 186 hosts, A and \hat{A} , respectively, following the approach of Kretzschmar and Adler (1993). The
 187 derivation of the VMR equations, and the general form that can be applied when other
 188 distributions such as the positive binomial or Neyman type-A are desired, can be found in
 189 Appendix B. If we proceed with the assumption that parasites are distributed according to
 190 the negative binomial, we can write the equations for the dynamic VMR as:

$$\begin{aligned} \frac{\partial A}{\partial t} = & \beta m \left(\frac{N + \hat{N}}{N} \right) + 2\rho + (1 - A) \left(\frac{\phi}{m} - \rho + \sigma + A\alpha \right) \\ & + \frac{\hat{N}\hat{m}}{Nm} \left[\theta \left(\hat{A}(3\hat{m} + 2\hat{A} - 1 - A - 2m) + (\hat{m} - m)^2 - A\hat{m} \right) \right. \\ & \left. + \gamma \left(\hat{m} + \hat{A} - A - 2m + \frac{m^2}{\hat{m}} \right) \right] \end{aligned} \quad (18)$$

$$\begin{aligned} \frac{\partial \hat{A}}{\partial t} - c \frac{\partial \hat{A}}{\partial x} = & 2\rho + (1 - \hat{A}) \left(\frac{\phi}{\hat{m}} - \rho + \sigma + \hat{A}(\alpha + \theta) \right) \\ & + \frac{Nm}{\hat{N}\hat{m}} \omega \left(m + A - \hat{A} - 2\hat{m} + \frac{\hat{m}^2}{m} \right) \end{aligned} \quad (19)$$

191 The complete system describing the spatial and temporal dynamics of hosts and parasites
 192 under the negative binomial assumption is described by equations (14-17) and (18-19).

193 **3. Simulations and results**

194 In this section, we illustrate how migration can affect parasite burden and the impor-
 195 tance of including a dynamically changing VMR using simulations of the host-macroparasite
 196 model introduced in section 2. In its basic form, the model captures the spatiotemporal
 197 disease dynamics along the migration corridor but does not consider the full annual migra-
 198 tion cycle, including overwintering and breeding. However, in section 3.4 we also illustrate
 199 how the model can be extended to consider breeding and overwintering seasons when a host

200 population is not migrating.

201 3.1. Simulation methods

202 We simulated the model over a discrete space-time grid using a numerical scheme that,
203 at each time step, split the problem between two different processes: (1) spatial dynamics
204 of moving populations and (2) temporal dynamics of birth, mortality, and switching move-
205 ment status. This approach is known as operator splitting in the numerical solution of
206 advection-diffusion-reaction equations (Hundsdoerfer and Verwer, 2013). We assumed Neu-
207 mann boundary conditions, but considered a migration corridor that was long enough to
208 accommodate migrants who moved for the entire duration of the migration season. An al-
209 ternative approach that may be more appropriate in certain systems would be to consider
210 the end of the migration at a certain point in space, with an absorbing boundary. For details
211 of our numerical methods, see Appendix C.

212 The model we have described is general and different parameterizations make it adaptable
213 to a variety of life-histories of both the parasite and host. For our initial exploration of the
214 dynamics, we considered a theoretical population migrating 2000 km along a one-dimensional
215 migration corridor, with a spatial grid consisting of steps $\Delta x = 1$ km in length. First, we
216 consider the migratory season only when hosts have left their breeding grounds and therefore
217 host reproduction is $\beta = 0 \text{ yr}^{-1}$. In section 3.4, we consider $\beta > 0$ during a breeding season.
218 Other parameters were varied from their baseline values (Table 2) in sensitivity analyses
219 exploring their effect on the dynamics, with details given in the relevant sections below. The
220 migration period lasted 0.2 yr (or 73 days), simulated using a time step of $\Delta t = 0.0001$ yr.

221 We initiated all simulations with a host population that had a peak abundance of 1000
222 individuals at the start of the migration (arbitrarily set at 130 km) and a Gaussian spatial
223 distribution with a standard deviation of 30 km. We added one individual to both the initial
224 moving and stationary host populations to ensure the problem was well posed; we required
225 that N and P be positive in order to define m and A (Appendix A) and to avoid numerical
226 issues when host abundance was zero due to the ratios in equations (18-19). This meant

227 that host abundance was never exactly zero in our simulations. We assumed an initial
228 parasite burden of $m(x, 0) = \hat{m}(x, 0) = 5$ parasites per stationary and moving host with
229 overdispersion of $k = 0.8$, giving a VMR of $A(x, 0) = \hat{A}(x, 0) = 7.25$. The initial density of
230 free-living parasites was $L(x, 0) = 1 \text{ km}^{-1}$.

231 *3.2. Parasite burden of moving and stationary populations*

232 We contrasted the parasite dynamics of non-migratory and migratory host populations
233 with the production of free-living parasites ranging from $\kappa = 0$ to $\kappa = 10 \text{ parasite}^{-1} \text{ yr}^{-1}$ and
234 the within-host reproduction ranging from $\rho = 0$ to $\rho = 10 \text{ parasite}^{-1} \text{ yr}^{-1}$. We hypothesized
235 that increases in ρ would affect parasite burdens of stationary and migrating hosts in a similar
236 way because within-host reproduction of parasites would track movement of migratory hosts.
237 In contrast, increases in κ would emphasize any differences in parasite dynamics between
238 stationary and migrating hosts because migratory hosts will move away from areas where
239 free-living parasites accumulate.

240 For these simulations, we set $\gamma = \omega = 0$ and $\theta = 0$ so that hosts did not switch between
241 stationary and moving. The initial non-migratory host population was entirely stationary
242 and remained so throughout the simulation. The initial migratory host population was
243 entirely moving and therefore migrated at the constant speed c for the duration of the
244 simulation. We report the host abundance, parasite burden, VMR, and density of free-living
245 parasites after 0.2 yr for the non-migratory and migratory populations (Fig. 1). These
246 variables correspond to the stationary and moving populations for the non-migratory and
247 migratory simulations, respectively, because hosts were not allowed to switch movement
248 status in these simulations.

249 The effect of increasing within-host parasite production had similar effects for non-
250 migratory and migratory populations, as we predicted. As ρ increased, host populations
251 declined more rapidly (Fig. 2a), parasite burdens increased more rapidly (Fig. 2b), and
252 parasites were more aggregated among hosts (Fig. 2c). The build-up of free-living parasites
253 at the location of the non-migratory host population was higher (Fig. 2d) and resulted in

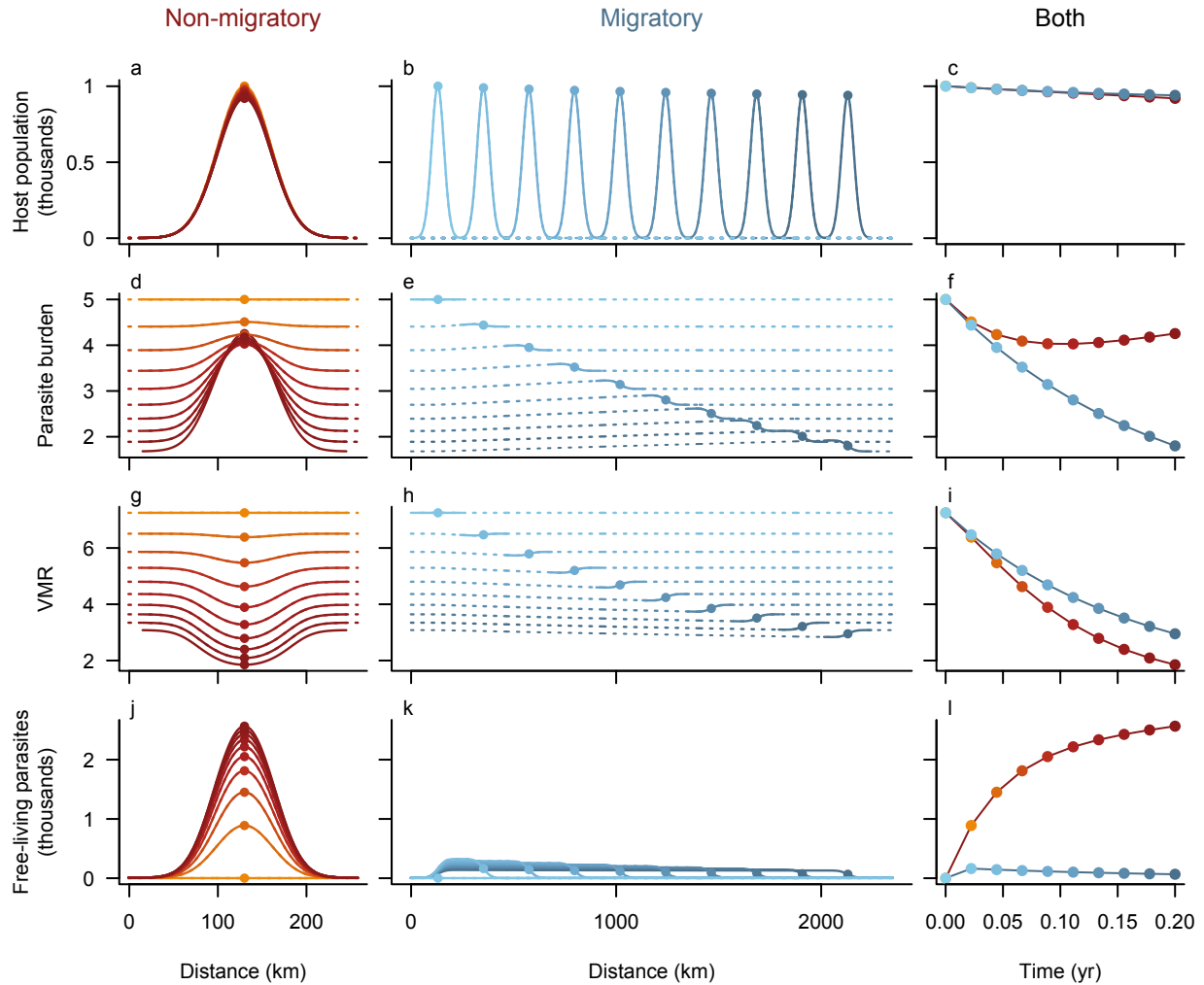


Figure 1: Host abundance for a non-migratory population (a; red) and a migratory host population that migrates 2000 km (b; blue) from $t = 0$ (orange/light blue) to $t = 0.2$ yr (dark red/blue). Parasite burdens declined in both cases but were much lower at the end of the migration season for migratory populations (e) than non-migratory populations (d), due to migratory escape from the buildup of free-living parasites (j,k). Dotted lines correspond to regions in space where host abundance was less than one individual. The change over time in variables at peak host abundance is shown on the right, emphasizing differences between migratory (red) and non-migratory (blue). Parameters for the simulation are given in Table 2, with the exception of $\omega = 0$, $\gamma = 0$, $\rho = 0$, and $\kappa = 10$. See https://rawgit.com/sjpeacock/Migration_model/master/MigVsStat.html for an animated version.

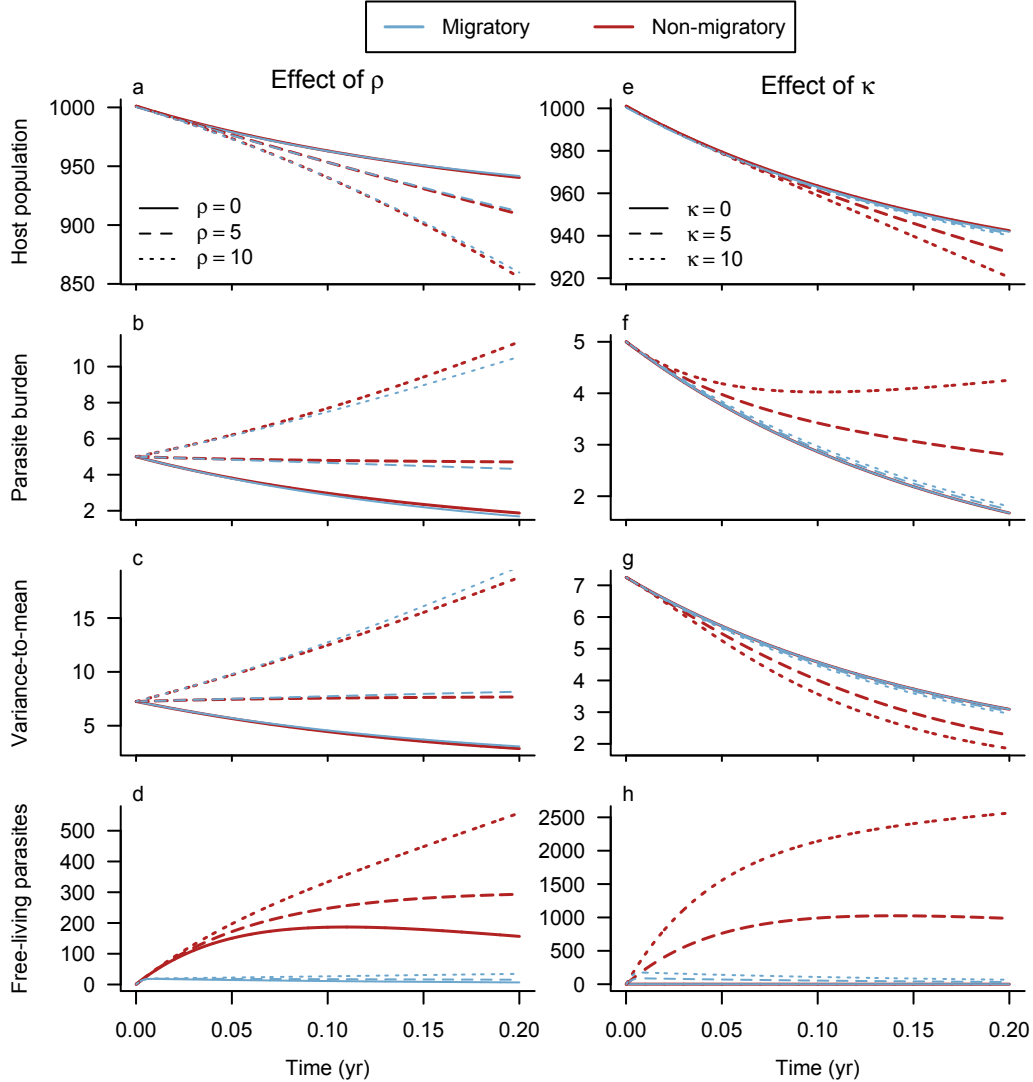


Figure 2: The host population (a,e), parasite burden (b,f), VMR (c,g), and density of free-living parasites over time for increasing within-host parasite reproduction (ρ , left) and production of free-living parasites (κ , right). As for the right-hand column of Fig. 1, dark red lines correspond to the non-migratory populations at the initial location $x_0 = 130$ km and the lighter blue lines correspond to the migrating populations at the location of peak host abundance (i.e., $x(t) = x_0 + ct$).

254 slightly higher parasite burdens on non-migratory hosts than on migratory hosts.
 255 Increases in κ also led to lower host densities, but the effect was much larger for non-
 256 migratory hosts (Fig. 2e). Parasite burden was higher for non-migratory hosts than migra-
 257 tory hosts when $\kappa > 0$ (Fig. 1, Fig. 2f). While increasing ρ resulted in a higher VMR (Fig.
 258 2c), increasing κ had the opposite effect (Fig. 2g); parasites were less aggregated because
 259 infection by free-living parasites occurred at random, evening out the parasite distribution

260 among hosts. The simultaneous decline in host population (Fig. 2e), parasite burden (Fig.
 261 2f), and VMR (Fig. 2g) for both non-migratory and migratory populations suggest that
 262 the most heavily infected hosts are suffering parasite-induced mortality. The VMR declined
 263 more rapidly for non-migratory hosts than migratory hosts as κ increased (Fig. 2g) due to
 264 parasite-induced mortality culling heavily infected individuals. For non-migratory popula-
 265 tions, new infections may have been more important in lowering the VMR as the exposure
 266 to free-living parasites was much higher for non-migratory hosts (Fig. 2h).

267 3.3. *Effect of dynamic variance-to-mean ratio*

268 Kretzschmar and Adler (1993) were the first to consider modelling the VMR as an addi-
 269 tional dynamic variable. They found that hosts and parasites coexist at a stable equilibrium
 270 only if the VMR increases with increasing mean of the parasite distribution, due to the
 271 associated increase in per capita parasite death with higher parasite loads. However, they
 272 also found that in cases with very strong aggregation, parasites may be unable to effectively
 273 control the host population and the system is unstable. Therefore, if one wishes to say some-
 274 thing about stability, it is necessary to include the VMR as a dynamic variable whenever
 275 parasite burden affects host survival (and therefore parasite survival). But what about our
 276 migratory model, where it is the transient dynamics during a migration season that are of
 277 interest? How does a dynamic VMR affect parasite burdens and host densities compared to
 278 simpler models?

279 To answer this question, we compared simulations using three variants of the model: (1)
 280 assuming a **Poisson** distribution of parasites among hosts where the variance was always
 281 equal to the mean (i.e., $A(x, t) = \hat{A}(x, t) = 1$ and $k \rightarrow \infty$), (2) assuming a negative binomial
 282 distribution of parasites among hosts with a **constant aggregation** parameter of $k = 0.8$
 283 such that $A(x, t) = m(x, t)/k + 1$ and $\hat{A}(x, t) = \hat{m}(x, t)/k + 1$, and (3) the full model
 284 accounting for **dynamic VMR** given by equations (18-19). In a spatial context, we were
 285 most interested in how these models compared when parasites had a strong influence on the
 286 rate of host stopping. Therefore, we compared simulations under baseline parameter values

287 (Table 2) with the exception of the per-parasite increase in stopping which we set at $\theta = 10$.

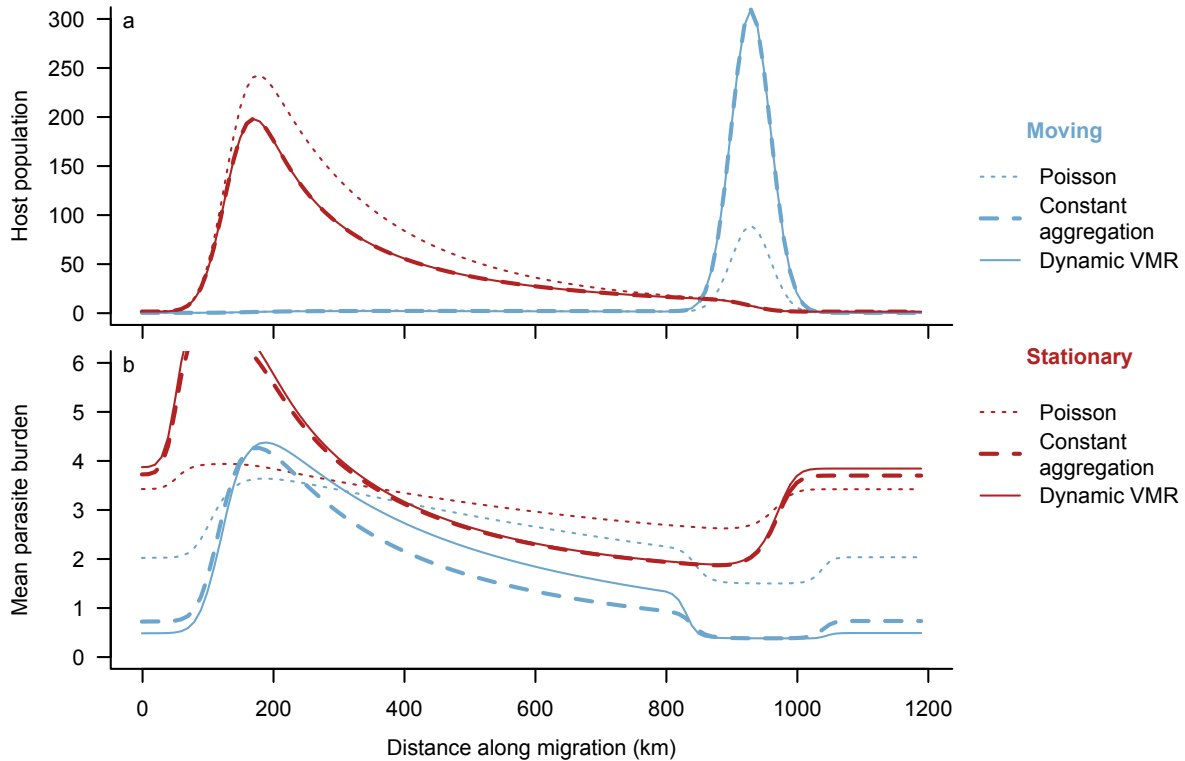


Figure 3: The spatial distribution of moving and stationary hosts (a; $\hat{N}(x, t)$ and $N(x, t)$, respectively) and their respective mean parasite burdens (b; $\hat{m}(x, t)$ and $m(x, t)$), part-way through a migration at $t = 0.08$ yr (approx. 30 days). The full model given by equations (18-19) was simulated but the solutions for VMR and the density of infectious parasite larvae in the environment are not shown. The per-parasite increase in the rate of stopping was high ($\theta = 10$), resulting in much of the host population being left behind and a lower parasite burden on those hosts that continue to migrate. All other parameters were at their baseline values (Table 2).

288 For each variant of the model, the parasite burden was always higher on stationary hosts
 289 than on moving hosts due to the tendency for infected hosts to have higher rates of stopping
 290 (Fig. 3b). This parasite-induced migratory stalling also lead to a relatively high abundance
 291 of stationary hosts at the start of the migration, where parasite burdens were highest, and a
 292 long-tail that extended behind the moving population as hosts stopped along the migration
 293 route.

294 The Poisson distribution lead to the lowest host abundance (Fig. 3a) and the highest
 295 mean parasite burden (Fig. 3b) for the moving population. Under the Poisson model,

296 parasites are more evenly distributed among hosts and so the prevalence of infection is higher
297 for a given mean parasite burden. Thus, a larger proportion of the host population will
298 experience an increase in stopping rates, leading to fewer moving hosts. Further, parasite-
299 induced stopping will be less effective at reducing the mean parasite burden of moving hosts,
300 leading to higher mean parasite burdens among moving hosts.

301 The constant aggregation and dynamic VMR models predicted very similar host densities
302 along the migration (Fig. 3a), but there were slight differences in the parasite burdens (Fig.
303 3b). As might be expected when migratory ability depends on parasite load, the dynamic
304 VMR model predicted higher parasite burdens at the trailing edge of the moving population,
305 and lower parasite burden at the centre and leading edge of the moving population.

306 *3.4. Annual dynamics*

307 Thus far, we have focused on migration and ignored host reproduction and natural mor-
308 tality. In many systems, hosts will migrate between breeding and overwintering grounds and
309 parameters in the model may differ among these seasons. To illustrate how the model can be
310 used to understand host-parasite dynamics over an annual cycle, we combined simulations
311 using different parameters for each of four seasons within a year: breeding, fall migration,
312 overwintering, and spring migration. During the breeding and overwintering seasons, we
313 assumed that all hosts were stationary with $\gamma = \omega = 0$ so that no hosts switched to migrat-
314 ing. During the breeding season, hosts reproduced at rate $\beta = 2.5 \text{ yr}^{-1}$, and for all other
315 seasons we set $\beta = 0 \text{ yr}^{-1}$. At the beginning of the migration seasons, all hosts switched
316 from stationary to moving at speed $c = 10000 \text{ km yr}^{-1}$. At the end of migration seasons,
317 moving hosts and their parasites switched back to stationary wherever they were when the
318 migration season ended, and remained there for the following breeding or overwintering sea-
319 son. We ignored stopping, starting, and migratory stalling, keeping $\gamma = \omega = 0$ and $\theta = 0$
320 for simplicity (this assumption could be relaxed in future analyses). Other parameters were
321 set at their baseline values (Table 2) except for the mortality of free-living parasites, which
322 we varied from $\mu_L = 0.5$ to the baseline value of $\mu_L = 5$ and host mortality which was

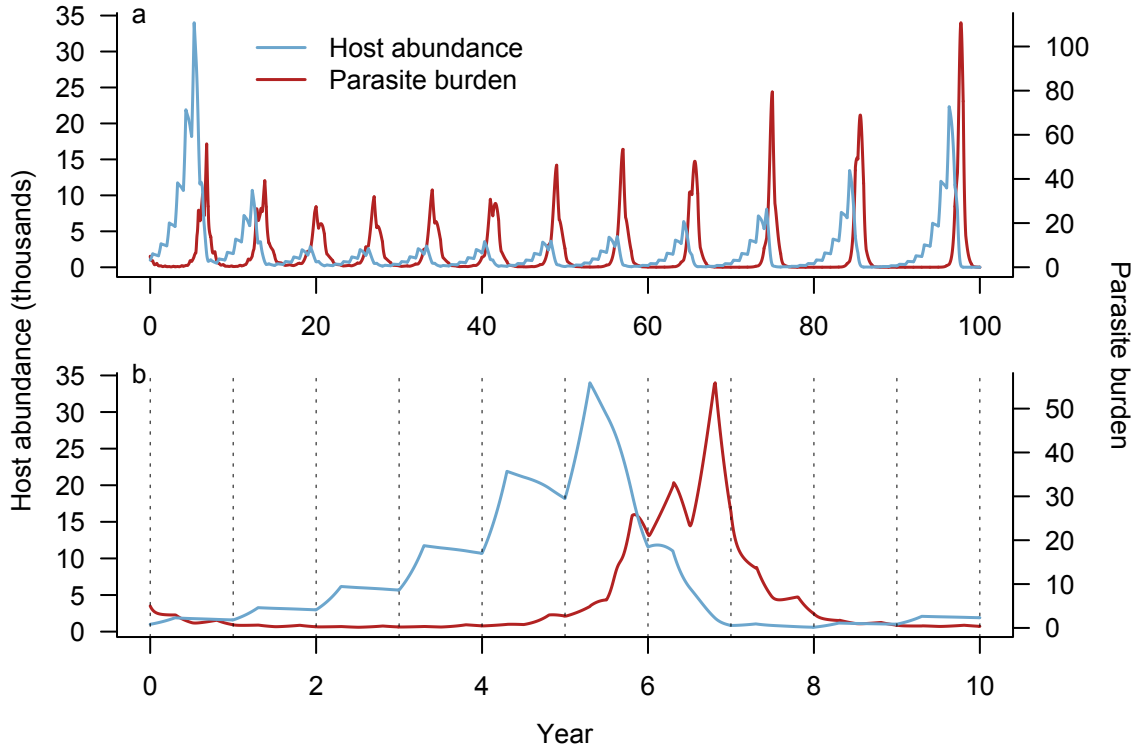


Figure 4: The host abundance (light blue; left axis) and parasite burden (dark red; right axis) over a 100-year simulation including breeding, migration, and overwintering seasons. Over long time-scales, the dynamics are cyclic with a period of ~ 8 years (a). Zooming in on the first decade (b), we also observe fluctuations within a year, with host abundance peaking after the breeding season and parasite burden rising during breeding and overwintering, and declining during migrations. Parameters were at baseline values (Table 2) except host birth and natural host death which changed with season (see main text for details).

323 highest during migration ($\mu_L = 0.1$) and lowest during the breeding season ($\mu = 0.05$) with
 324 overwintering intermediate between those two ($\mu_L = 0.08$).

325 We report the host abundance and parasite burden over a 100-year simulation at the
 326 location of peak host abundance in space. The peak host abundance was centred at the
 327 breeding grounds during the breeding season (i.e., 130 km along the spatial corridor), at the
 328 overwintering grounds during the overwintering season (i.e., 2130 km), and moved in between
 329 those two locations during the migration seasons. At baseline parameter values (Table 2), we
 330 observed cyclic dynamics in host abundance and parasite burden with a period of ≈ 8 years
 331 (Fig. 4a). Parasite burden tended to lag a year or so behind host abundance, which has also
 332 been observed in previous host-macroparasite models that display cyclic dynamics (Dobson

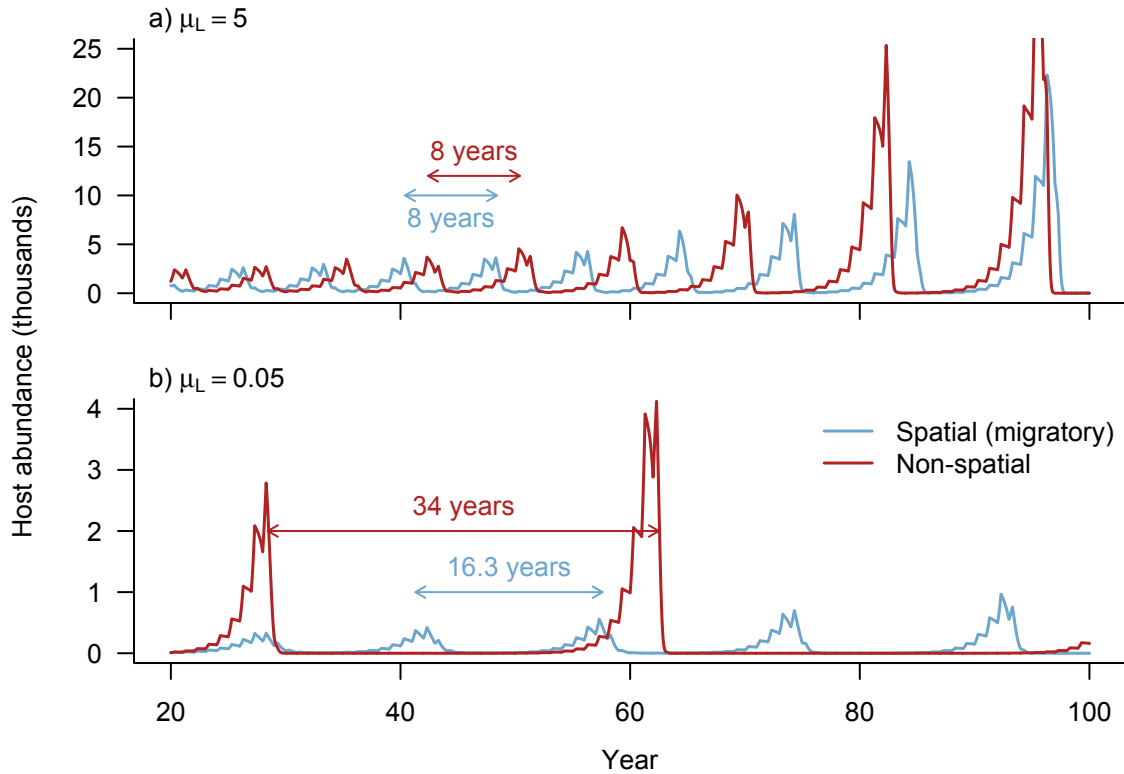


Figure 5: The host abundance over the last 80 years of a 100-year simulation using a model for a migratory population that experienced breeding, migration, and overwintering seasons (light blue lines) and a non-spatial model where all parameters were the same but hosts did not migrate (dark red lines). The period of cycles in the non-spatial model were similar when the mortality of free-living parasites was high ($\mu_L = 5$, b), but differed when mortality of free-living parasites was low ($\mu_L = 5$, d).

333 and Hudson, 1992). Within a given year, we saw an increase in host abundance during the
 334 breeding season and a decline in host abundance throughout the rest of the year due to
 335 natural and parasite-induced mortality (Fig. 4b). During the first decade of the simulations,
 336 the parasite burden increased during the breeding season, declined during migration, and
 337 increased again during overwintering. However, over the longer term, this annual pattern did
 338 not hold (Fig. 4b), perhaps due to the buildup of free-living parasites along the migration
 339 route eroding some benefit of migratory escape.

340 To understand the effect of migration on multi-year host-parasite dynamics, we compared
 341 the dynamics of our spatially explicit migration model to the dynamics of the non-spatial
 342 model developed by Kretzschmar and Adler (1993) that was otherwise the same (i.e., included
 343 dynamic VMR). For the non-spatial simulations, we still assumed four seasons within the

344 year but the “migratory” seasons did not include the movement of hosts. This altered the
345 dynamics in that the density of free-living parasites that hosts encountered only changed
346 due to host and parasite dynamics but not due to host movement away from larval patches
347 as for the spatial model. We used the same parameterization as for spatial model in order
348 to isolate the effect of adding a spatial component on host-parasite dynamics.

349 Predictions from the non-spatial model showed similar qualitative behaviour as our spa-
350 tial model when the mortality of free-living parasites was high; populations underwent cycles
351 with approximately the same amplitude and period whether or not spatially explicit migra-
352 tion was included (Fig. 5a). When the mortality of free-living parasites was low, both models
353 predicted lower host abundances (Fig. 5b), likely due to a higher abundance of free-living
354 parasites in the environment regulating host populations. However, our spatial model pre-
355 dicted lower and more frequent peaks in host abundance than the non-spatial model (Fig.
356 5b). The frequency of cycles was more similar to the high μ_L scenario than for the non-
357 spatial model, likely because the migration away from infection hotspots mitigated the effect
358 of low free-living parasite mortality. Conversely, in the non-spatial model, hosts could not
359 move away from high densities of free-living parasites that accumulate when the mortality
360 of free-living parasites is low, and so the dynamics were quite different under low μ_L than
361 under high μ_L .

362 4. Discussion

363 Animal migrations may have profound implications for parasite dynamics in wildlife by
364 spreading parasites to new areas, allowing hosts to escape infection hotspots, or culling
365 infected individuals from host populations (Altizer et al., 2011). These mechanisms may
366 influence parasite burdens of migratory hosts in opposing ways, making it difficult to under-
367 stand the net effect of migration on animal health. We recognized a need for a modelling
368 framework that could incorporate host migration and macroparasite dynamics to predict the
369 conditions under which we might expect, for example, migratory escape from parasites. In

370 this paper, we developed such a framework and showed how it builds upon previous models
371 of host-parasite dynamics by explicitly accounting for parasite burden and aggregation, in-
372 cluding spatial dynamics, and allowing the distribution of parasites among hosts to change
373 dynamically in space and time.

374 Migration can be extremely taxing, and the extra cost of infection may compromise
375 a host's ability to keep up with the herd (Risely et al., 2017). Our analysis revealed a
376 phenomenon we have termed parasite-induced migratory stalling, whereby parasite-impacts
377 on migratory ability can lead to positive feedbacks in parasite transmission that may result
378 in the host population halting their migration. Our model is the first to have exhibited
379 this behavior because it includes two key features that previous models (e.g., Hall et al.,
380 2014; Johns and Shaw, 2015) were lacking: transmission dynamics during migration and
381 spatiotemporal dynamics of the parasite burden of hosts. These features allowed us to
382 explore how parasite-mediated increases in the rate that hosts stop moving affect migratory
383 ability and parasite burdens. When the rate of stopping increased with parasite burden, we
384 found that hosts tended to accumulate in the stationary category. In the case of parasites
385 that are environmentally transmitted, moving hosts can escape infection hotspots while
386 stationary hosts experience higher infection pressure. We also observed spatial structure in
387 the parasite burden even within the moving host population; hosts at the leading edge of
388 the migration tended to have lower parasite burdens than hosts at the trailing edge, while
389 stationary hosts had even higher parasite burdens. Our model simulations were not specific
390 to any biological system, but specific parameterizations could be adopted to understand, for
391 example, the potential for migratory stalling of birds at stopover sites, which tend to be
392 infection hotspots, or the risk of migratory stalling for wildlife in contact with domesticated
393 animals that can act as reservoir hosts.

394 Our model predictions are consistent with several empirical studies of parasite burdens
395 in migratory wildlife. In species that show partial migration, where only certain popula-
396 tions display migratory behaviour, sedentary populations often have higher parasite burdens

397 across taxa. For example, in Canada, migratory elk were less likely to be infected with the
398 trematode *Fascioloides magna* than resident populations (Pruvot et al., 2016). Similarly, the
399 migration of red deer in Norway was associated with lower tick abundance (Qviller et al.,
400 2013). The loss of migratory behaviour in certain populations of monarch butterflies in the
401 USA has led to higher prevalence of protozoan parasites than in migratory conspecifics
402 (Satterfield et al., 2015). Further studies have shown a negative relationship between the
403 distance migrated and parasite prevalence (e.g., Bartel et al., 2011). Globally, animal migra-
404 tions are under increasing pressure from anthropogenic environmental change with observed
405 declines in migratory behaviour (Wilcove and Wikelski, 2008). Quantitative models such as
406 ours allow scientists to predict the potential consequences for animal health.

407 Although limited in scope, the annual simulations illustrated how our model could be
408 used to understand seasonal effects of migration and host breeding on parasite dynamics,
409 and the long-term implications of seasonal or climatic changes in parameters such as the
410 mortality of free-living parasites. We found that host and parasite populations tended to
411 cycle on long timescales, but the exact period of oscillations depended on the mortality
412 of free-living parasites. Red grouse have classically illustrated such population cycles and
413 experimental studies have suggested that parasites may be the cause of these cycles (Hud-
414 son and Greenman, 1998), although other factors are likely also at play (Redpath et al.,
415 2006). Many wildlife populations display such cycles, including migratory species such as
416 caribou (Ferguson et al., 1998), leaving it open for future work to examine possible links
417 with parasitism. If parasites are contributing to population cycles, then our model simu-
418 lations suggest that changes to the mortality of free-living parasites due to, for example,
419 climate change (Dobson et al., 2015), may have important consequences for the period of
420 host population cycles. The presence of migratory behaviour tended to mitigate changes to
421 population cycles that resulted from reduced parasite mortality, suggesting that migratory
422 species might be more resilient to changes in parasite survival. Alternatively, higher survival
423 of free-living parasites combined with the loss of migratory behavior associated with global

424 anthropogenic change (Wilcove and Wikelski, 2008) could lead to dramatic changes in host
425 population cycles.

426 One important aspect of migration that is missing from our model is the collective be-
427 havior of migratory animals. We assume that an individual's movement depends on parasite
428 burden but is independent of what other animals in the herd, school, or flock are doing. In
429 reality, many animal groups move as a cohesive unit to avoid predation and increase foraging
430 efficiency (Alexander, 1974). Thus, a single individual with a high parasite burden may be
431 left behind, but perhaps healthy individuals would hang back if the prevalence of parasitism
432 in the herd was high. This kind of collective behavior may exacerbate the effect of migratory
433 stalling that we have described. Models with simple rules for attraction, repulsion, and ori-
434 entation among neighbours in a herd can reproduce the seemingly complex group dynamics
435 observed in nature (e.g., Couzin et al., 2002; Eftimie et al., 2007). Incorporating the effects
436 of parasites into these simple rules may provide insight into how collective dynamics would
437 affect the inferences we have made, and is an area for future research.

438 The model we have presented is a general framework for host-macroparasite dynamics
439 along a spatial domain, such as a migration corridor. Because of its generality, it can be
440 adapted to answer a number of important questions facing wildlife disease ecology. What
441 are the conditions under which we might expect migratory escape, migratory culling, or
442 migratory stalling? How might the effect of rising temperatures on developmental rates of
443 parasites and/or migration timing of hosts affect the health of migrating animals? More
444 than just changing parameters, the structure of the model can be adapted in various ways;
445 for example, to examine how reservoir hosts contributing free-living transmissive stages, such
446 as domestic animals, influence parasite dynamics of migrating wildlife. We have provided
447 the basic framework for these and other future studies that will shed light on how parasites
448 might affect wildlife populations in a changing world.

449 5. Acknowledgements

450 We thank Martin Krkošek for motivating discussions. The authors gratefully acknowledge
451 funding from an NSERC Vanier Scholarship and Postdoctoral Fellowship to SJP, NSERC
452 Discovery Grants to MAL and PKM, a Canada Research Chair to MAL, and a postdoctoral
453 fellowship from the Pacific Institute for Mathematical Sciences to JB.

454 6. Literature cited

- 455 Adler, F.R., Kretzschmar, M., 1992. Aggregation and stability in parasite-host models.
456 *Parasitology* 104, 199–205. doi:10.1017/S0031182000061631.
- 457 Alexander, R.D., 1974. The Evolution of Social Behavior. *Annual Review of Ecology and*
458 *Systematics* 5, 325–383. doi:10.1146/annurev.es.05.110174.001545.
- 459 Altizer, S., Bartel, R., Han, B.A., 2011. Animal Migration and Infectious Disease Risk.
460 *Science* 331 (6015), 296–302. doi:10.1126/science.1194694.
- 461 Anderson, R.M., May, R.M., 1978. Regulation and stability of host-parasite population
462 interactions: I. Regulatory processes. *Journal of Animal Ecology* 47 (1), 219–247.
- 463 Anderson, R.M., May, R.M., 1979. Population biology of infectious diseases: Part I. *Nature*
464 280 (5721), 361–367. doi:10.1038/280361a0.
- 465 Bartel, R.A., Oberhauser, K.S., De Roode, J.C., Altizer, S.M., 2011. Monarch butterfly
466 migration and parasite transmission in eastern North America. *Ecology* 92 (2), 342–351.
467 doi:10.1890/10-0489.1.
- 468 Bradley, C.A., Altizer, S., 2005. Parasites hinder monarch butterfly flight: implications for
469 disease spread in migratory hosts. *Ecology Letters* 8, 290–300. doi:10.1111/j.1461-0248.
470 2005.00722.x.

- 471 Cornell, S.J., Isham, V.S., Grenfell, B.T., 2004. Stochastic and spatial dynamics of nematode
472 parasites in farmed ruminants. *Proceedings of the Royal Society of London. Series B:*
473 *Biological Sciences* 271 (1545), 1243–1250. doi:10.1098/rspb.2004.2744.
- 474 Courant, R., Friedrichs, K., Lewy, H., 1967. On the partial difference equations of mathe-
475 matical physics. *IBM Journal* 11 (2), 215–234. doi:10.1147/rd.112.0215.
- 476 Couzin, I.D., Krause, J., James, R., Ruxton, G.D., Franks, N.R., 2002. Collective memory
477 and spatial sorting in animal groups. *Journal of Theoretical Biology* 218 (1), 1–11. doi:
478 10.1006/jtbi.2002.3065.
- 479 Dobson, A., Molnár, P.K., Kutz, S., 2015. Climate change and Arctic parasites. *Trends in*
480 *Parasitology* 31 (5), 181–188. doi:10.1016/j.pt.2015.03.006.
- 481 Dobson, A.P., Hudson, P.J., 1992. Regulation and stability of a free-living host-parasite
482 system: *Trichostrongylus tenuis* in red grouse. II. Population models. *Journal of Animal*
483 *Ecology* 61, 487–498.
- 484 Eftimie, R., de Vries, G., Lewis, M.a., Lutscher, F., 2007. Modeling Group Formation and
485 Activity Patterns in Self-Organizing Collectives of Individuals. *Bulletin of Mathematical*
486 *Biology* 69 (5), 1537–1565. doi:10.1007/s11538-006-9175-8.
- 487 Ferguson, M.A.D., Williamson, R.G., Messier, F., 1998. Inuit Knowledge of Long-Term
488 Changes in a Population of Arctic Tundra Caribou. *Arctic* 51 (3), 201–219.
- 489 Folstad, I., Nilssen, A.C., Halvorsen, O., Andersen, J., 1991. Parasite avoidance: the cause
490 of post-calving migrations in Rangifer? *Canadian Journal of Zoology* 69, 2423–2429.
- 491 Hall, R.J., Altizer, S., Bartel, R.A., 2014. Greater migratory propensity in hosts lowers
492 pathogen transmission and impacts. *Journal of Animal Ecology* 83, 1068–1077. doi:
493 10.1111/1365-2656.12204.

- 494 Hall, R.J., Brown, L.M., Altizer, S., 2016. Modeling vector-borne disease risk in migratory
495 animals under climate change. *Integrative and Comparative Biology* 56 (2), icw049. doi:
496 10.1093/icb/icw049.
- 497 Hudson, P., Greenman, J., 1998. Competition mediated by parasites: Biological and
498 theoretical progress. *Trends in Ecology and Evolution* 13 (10), 387–390. doi:10.1016/
499 S0169-5347(98)01475-X.
- 500 Hudson, P.J., Rizzoli, A.P., Grenfell, B.T., Heesterbeek, J.A.P., Dobson, A.P., 2002. *Ecology*
501 *of wildlife diseases*. Oxford University Press.
- 502 Hundsdorfer, W., Verwer, J.G., 2013. Numerical solution of time-dependent advection-
503 diffusion-reaction equations, volume 33. Springer Science & Business Media.
- 504 Johns, S., Shaw, A.K., 2015. Theoretical insight into three disease-related benefits of migra-
505 tion. *Population Ecology* 58, 213. doi:10.1007/s10144-015-0518-x.
- 506 Kretzschmar, M., Adler, F.R., 1993. Aggregated distributions in models for patchy popula-
507 tions. *Theoretical Population Biology* 43, 1–30.
- 508 Krkošek, M., Connors, B.M., Ford, H., Peacock, S., Mages, P., Ford, J.S., Morton, A., Volpe,
509 J.P., Hilborn, R., Dill, L.M., Lewis, M.A., 2011. Fish farms, parasites, and predators:
510 implications for salmon population dynamics. *Ecological Applications* 21 (3), 897–914.
511 doi:10.1890/09-1861.1.
- 512 Krkošek, M., Gottesfeld, A., Proctor, B., Rolston, D., Carr-Harris, C., Lewis, M.A., 2007.
513 Effects of host migration, diversity and aquaculture on sea lice threats to Pacific salmon
514 populations. *Proceedings of the Royal Society B* 274 (1629), 3141–3149. doi:10.1098/rspb.
515 2007.1122.
- 516 Kutz, S.J., Checkley, S., Verocai, G.G., Dumond, M., Hoberg, E.P., Peacock, R., Wu, J.P.,
517 Orsel, K., Seegers, K., Warren, A.L., Abrams, A., 2013. Invasion, establishment, and

518 range expansion of two parasitic nematodes in the canadian arctic. *Global Change Biology*
519 19 (11), 3254–3262. doi:10.1111/gcb.12315.

520 Lutscher, F., 2002. Modeling alignment and movement of animals and cells. *Journal of*
521 *Mathematical Biology* 45 (3), 234–260. doi:10.1007/s002850200146.

522 May, R.M., 1978. Host-Parasitoid Systems in Patchy Environments: A Phenomenological
523 Model. *Journal of Animal Ecology* 47 (3), 833–844.

524 May, R.M., Anderson, R.M., 1991. *Infectious Diseases of Humans*. Oxford University Press,
525 Oxford.

526 Milner, F.A., Zhao, R., 2008. A deterministic model of schistosomiasis with spatial structure.
527 *Mathematical Biosciences and Engineering* 5 (3), 505–522. doi:10.3934/mbe.2008.5.505.

528 Morgan, E.R., Medley, G.F., Torgerson, P.R., Shaikenov, B.S., Milner-Gulland, E.J., 2007.
529 Parasite transmission in a migratory multiple host system. *Ecological Modelling* 200 (3-4),
530 511–520. doi:10.1016/j.ecolmodel.2006.09.002.

531 Nendick, L., Sackville, M., Tang, S., Brauner, C.J., Farrell, A.P., 2011. Sea lice infection
532 of juvenile pink salmon (*Oncorhynchus gorbuscha*): effects on swimming performance and
533 postexercise ion balance. *Canadian Journal of Fisheries & Aquatic Sciences* 68 (2), 241–
534 249. doi:10.1139/F10-150.

535 Pruvot, M., Lejeune, M., Kutz, S., Hutchins, W., Musiani, M., Massolo, A., Orsel, K., 2016.
536 Better Alone or in Ill Company? The Effect of Migration and Inter-Species Comingling
537 on *Fascioloides magna* Infection in Elk. *Plos One* 11 (7), e0159319. doi:10.1371/journal.
538 pone.0159319.

539 Qviller, L., Risnes-Olsen, N., Bærum, K.M., Meisingset, E.L., Loe, L.E., Ytrehus, B., Vilju-
540 grein, H., Mysterud, A., 2013. Landscape Level Variation in Tick Abundance Relative to
541 Seasonal Migration in Red Deer. *PLoS ONE* 8 (8). doi:10.1371/journal.pone.0071299.

- 542 Redpath, S.M., Mougeot, F., Leckie, F.M., Elston, D.A., Hudson, P.J., 2006. Testing the
543 role of parasites in driving the cyclic population dynamics of a gamebird. *Ecology Letters*
544 9 (4), 410–418. doi:10.1111/j.1461-0248.2006.00895.x.
- 545 Riley, S., Eames, K., Isham, V., Mollison, D., Trapman, P., 2015. Five challenges for spatial
546 epidemic models. *Epidemics* 10, 68–71. doi:10.1016/j.epidem.2014.07.001.
- 547 Risely, A., Klaassen, M., Hoye, B.J., 2017. Migratory animals feel the cost of getting sick: a
548 meta-analysis across species. *Journal of Animal Ecology* In press. doi:10.1111/ijlh.12426.
- 549 Salsa, S., 2015. *Partial differential equations in action*, volume 86. Springer-Verlag, Milan,
550 Italy, second edition. doi:10.1007/978-3-319-15093-2.
- 551 Satterfield, D.A., Maerz, J.C., Altizer, S., 2015. Loss of migratory behaviour increases
552 infection risk for a butterfly host. *Proceedings of the Royal Society B: Biological Sciences*
553 282, 20141734. doi:10.1098/rspb.2014.1734.
- 554 Shaw, D.J., Grenfell, B.T., Dobson, A.P., 1998. Patterns of macroparasite aggregation in
555 wildlife host populations. *Parasitology* 117, 597–610. doi:10.1017/S0031182098003448.
- 556 Wilcove, D.S., Wikelski, M., 2008. Going, going, gone: Is animal migration disappearing?
557 *PLoS Biology* 6 (7), 1361–1364. doi:10.1371/journal.pbio.0060188.

558 **Appendix A. Well posedness and positivity**

559 In this appendix, we prove the well posedness and positivity of the solution to equations
 560 (1-5) and show the existence of N , m , and A and their moving counterparts. We start by
 561 considering the problem posed by equations (1-5), but instead of considering i up to an
 562 infinite number of parasites, we assume that the number of parasites per host is bounded
 563 by some large number I (e.g., the carrying capacity for macroparasites on hosts). Equations
 564 (1-5) then become:

$$\left\{ \begin{array}{l}
 \frac{\partial p_0}{\partial t} = \beta \sum_{i=0}^I (p_i + \hat{p}_i) - (\mu + \lambda L + \omega)p_0 + \sigma p_1 + \gamma \hat{p}_0 \\
 \frac{\partial p_i}{\partial t} = (\lambda L + \rho(i-1))p_{i-1} - (\mu + \lambda L + i(\alpha + \sigma + \rho) + \omega)p_i + \sigma(i+1)p_{i+1} + (\gamma + i\theta)\hat{p}_i \\
 \frac{\partial p_I}{\partial t} = (\lambda L + \rho(I-1))p_{I-1} - (\mu + \lambda L + I(\alpha + \sigma + \rho) + \omega)p_I + (\gamma + I\theta)\hat{p}_I \\
 \frac{\partial \hat{p}_0}{\partial t} + c \frac{\partial \hat{p}_0}{\partial x} = \omega p_0 - (\mu + \lambda L + \gamma)\hat{p}_0 + \sigma \hat{p}_1 \\
 \frac{\partial \hat{p}_i}{\partial t} + c \frac{\partial \hat{p}_i}{\partial x} = (\lambda L + \rho(i-1))\hat{p}_{i-1} - (\mu + \lambda L + i(\alpha + \sigma + \rho) + \gamma + i\theta)\hat{p}_i + \omega p_i + \sigma(i+1)\hat{p}_{i+1} \\
 \frac{\partial \hat{p}_I}{\partial t} + c \frac{\partial \hat{p}_I}{\partial x} = (\lambda L + \rho(I-1))\hat{p}_{I-1} - (\mu + \lambda L + I(\alpha + \sigma + \rho) + \gamma + I\theta)\hat{p}_I + \omega p_I \\
 \frac{\partial L}{\partial t} = \kappa \sum_{i=1}^I i(p_i + \hat{p}_i) - \mu_L L - \lambda L \sum_{i=0}^I I p_i + \hat{p}_i
 \end{array} \right. \tag{A.1}$$

565 for all $x \in \Omega = \mathbb{R}$, $t > 0$, $i \in \{1, \dots, I-1\}$, for some $I \in \mathbb{N}$ large enough, with the initial
 566 conditions $p_i(0, x) = p_i^0(x)$, $\hat{p}_i(0, x) = \hat{p}_i^0(x)$, and $L(0, x) = L^0(x)$ given for all $i \in \{0, \dots, I\}$
 567 such that p_i^0 , \hat{p}_i^0 and L^0 are non-negative, continuously differentiable, and integral in \mathbb{R} . More
 568 assumptions on the positivity of the initial conditions follow.

569 First, we prove the local existence of problem (A.1) and the uniqueness of a maximal so-
 570 lution, satisfying the initial condition (and boundary condition, when needed) using classical
 571 arguments as in Salsa (2015, Section 11.2.2) and Lutscher (2002). Then we prove that when
 572 they exist, the solutions are non-negative (assuming the initial conditions are non-negative)
 573 and can not blow up in time. This will prove the existence and uniqueness of a global so-
 574 lution. Using the Gronwall Lemma, we prove that each p_i is bounded from below by an

575 exponential function in time, which proves that as soon as the initial condition is positive,
 576 the solution is positive for all time. We then deduce that $N > 0$, $\hat{N} > 0$, $P > 0$, $\hat{P} > 0$ and
 577 m , \hat{m} , A , and \hat{A} are well defined for all time.

578 *Appendix A.1. Existence and uniqueness of the solutions for small time*

579 Using the methods of characteristics and the Banach fixed point theorem (see Sec-
 580 tion 11.2.2 of Salsa, 2015; Lutscher, 2002), we prove that there exists a smooth solution
 581 $(p_0, p_1, \dots, p_I, \hat{p}_0, \dots, \hat{p}_I, L)$ defined on some interval $[0, T_1]$ for T_1 small enough.

582 One starts by considering the problem along the characteristics. To make things clearer
 583 we will denote by $\underline{u} = (u_0, \dots, u_I, u_{I+1}, \dots, u_{2I+1}, u_{2I+2}) = (p_0, \dots, p_I, \hat{p}_0, \dots, \hat{p}_I, L)$ and
 584 define $\underline{c} = (c_0, \dots, c_{2I+2}) = (0, \dots, 0, c, \dots, c, 0)$ as the migration speed associated with
 585 each u_i . Now for each $i \in \{0, \dots, 2I + 2\}$, let $x_i(t) = \underline{c}_i t + \text{constant}$. Then, denoting
 586 $v_i(t) := u_i(t, x_i(t))$, v_i solves the following ODE:

$$\dot{v}_i = f_i(\underline{u}(t, x_i(t))) \quad (\text{A.2})$$

587 with f_i being the reaction term of u_i in problem (A.1). The \cdot on v_i stands for the derivative
 588 with respect to time. Integrating equation (A.2) with respect to time, we obtain for each i

$$u_i(t, x_i(t)) = u_i(0, x_i(0)) + \int_0^t f(\underline{u}(s, x_i(s))) ds. \quad (\text{A.3})$$

589 Notice that this argument can be adapted if $x \in \Omega \subsetneq \mathbb{R}$ and instead of going from 0 to t
 590 on the right hand side above, we will go from t_0 to t with $x_i(t_0)$ on the left boundary of
 591 the domain (as the population migrate from left to right). Let $C^0((0, T_1), B(u^0, \beta))$ be the
 592 set of continuous function defined for all $t \in [0, T_1]$, taking its values in the ball centred at
 593 u^0 , a continuous function, with radius $\beta > 0$. Then the second step is to prove that there
 594 exists some $\beta, T_1 > 0$ such that if $\underline{u} \in (C^0((0, T_1), B(u^0, \beta)))^m$, with $m = 2I + 2$, then the
 595 right hand side of (A.3) also belongs to $(C^0((0, T_1), B(u^0, \beta)))^m$. We know that f is locally

596 Lipschitz, thus for all $u_0 \in (B(0, \beta))^m$ and $u \in (B(u^0, \beta))^m$, there exists $k_\beta > 0$ such that

$$\|f(\underline{u})\| \leq k_\beta \|\underline{u}\| \leq k_\beta \cdot 2\beta := M. \quad (\text{A.4})$$

597 Choose $T_1 = \beta/M (= 1/(2 \cdot k_\beta))$, then for all $t \in (0, T_1)$,

$$u_i(0, x_i(0)) + \int_0^t f(u(s, x_i(s))) ds \in B(u^0, \beta). \quad (\text{A.5})$$

598 Moreover, with the same choice of T_1 above, one can prove that $u \mapsto u(0, x_i(0)) + \int_0^t f(u(s, x(s)))$
 599 is a contraction. Using the Banach fixed point theorem, we obtain the existence and unique-
 600 ness of the maximal solution of problem (A.1) defined for all $t \in (0, T)$, for some $T > 0$ and
 601 $x \in \mathbb{R}$ (or $\Omega \subsetneq \mathbb{R}$).

602 One has thus proved the existence and uniqueness of a maximal *mild* solution of our
 603 problem defined for all $t \in (0, T)$, for some $T > 0$, and for all $x \in \mathbb{R}$. To prove the existence
 604 of a classical solution (that is, a solution in C^1), one can use the same argument with the
 605 initial condition (and boundary condition if $\Omega \subsetneq \mathbb{R}$) in C^1 and $f \in C_{\text{loc}}^{1,1}$ and prove that the
 606 solution is integrable on \mathbb{R} for all $t \in (0, T)$, for some $T > 0$ (as we assumed that the initial
 607 condition is integrable). Now one needs to prove that the solution of problem (A.1) exists
 608 for all time $t \in \mathbb{R}^+$, that is the solution can not blow up in finite time.

609 *Appendix A.2. Existence, uniqueness, and non-negativity of the solutions for all time*

610 First notice that all the components of the problem u_i , $i \in \{0, \dots, 2I + 2\}$ stay non-
 611 negative if the initial condition is non-negative. Indeed, if u_i touches 0 and all the other
 612 functions u_j , $j \neq i$ stay non-negative, then $\frac{d}{dt} u_i(t, x_i(t)) \geq 0$ and thus u_i stays non-negative.
 613 This argument can be applied to all u_i , $i \in \{0, \dots, 2I + 2\}$ to prove the non-negativity of
 614 our system. Now one can study the behaviour of the total abundance of hosts at (x, t) ,
 615 considering

$$\bar{N} = \sum_{i=0}^I p_i + \hat{p}_i \quad (\text{A.6})$$

616 and then

$$\bar{N}(t) = \int_{\Omega} \bar{N}(t, x) dx < \infty \quad (\text{A.7})$$

Summing and integrating the PDEs from (A.1) we obtain that

$$\begin{aligned} \frac{d\bar{N}}{dt} &= - \int_{\Omega} \underline{c} \cdot \sum_{i=0}^I \partial_x \hat{p}_i(t, x) dx \\ &\quad - \int_{\Omega} (\mu - \beta) \sum_{i=0}^I (p_i(t, x) + \hat{p}_i(t, x)) dx \\ &\quad - \int_{\Omega} \left[(\lambda L + I\rho)(p_I(t, x) + \hat{p}_I(t, x)) + \alpha \sum_{i=1}^I i(p_i(t, x) + \hat{p}_i(t, x)) \right] dx \end{aligned} \quad (\text{A.8})$$

617 Using the regularity of the solution, we know that for all $t \in \mathbb{R}^+$, $-\int_{\Omega} \underline{c} \cdot \sum_{i=0}^I \partial_x \hat{p}_i(t, x) dx = 0$,
 618 when $\Omega = \mathbb{R}$. In the case of bounded domain, for Dirichlet boundary conditions or periodic
 619 boundary conditions, the first term on the right-hand side is equal to or less than zero and
 620 because of the non-negativity of the solution we get

$$\frac{d\bar{N}}{dt} \leq -(\mu - \beta)\bar{N}(t). \quad (\text{A.9})$$

621 Using Gronwall Lemma we obtain that

$$\bar{N}(t) \leq \bar{N}(0)e^{-(\mu-\beta)t} \quad (\text{A.10})$$

622 which yields, for each $i \in \{0, \dots, 2I + 1\}$, $u_i(t, x) \leq \bar{N}(0)e^{-(\mu-\beta)t}$ for all $t \geq 0$, $x \in \Omega$. This
 623 proves that the solution of problem (A.1) can not blow up in time and it is thus global in
 624 time, in the sense that there exists a unique maximal solution of problem (A.1) that exists
 625 for all $t > 0$, $x \in \Omega$.

626 Moreover, notice that as soon as $\beta < \mu$ we obtain that \bar{N} is decreasing in time and thus
 627 for all $i \in \{0, \dots, 2I + 1\}$

$$u_i(t, x) \leq \bar{N}(0) \quad (\text{A.11})$$

628 That is for all $i \in \{0, \dots, I\}$, p_i and \hat{p}_i are bounded for all $t \geq 0$, $x \in \Omega$.

629 *Appendix A.3. Positivity of the solutions*

630 Using the same argument as in previous subsection, we can prove that for all $t > 0$, $x \in \Omega$

$$L(t, x) \leq f(t) \tag{A.12}$$

631 with f being a positive function defined for all $t > 0$. Then using equations (A.1) we obtain

632 for each $i \in \{0, \dots, I\}$,

$$\frac{\partial p_i}{\partial t} \geq -(\mu + f(t) + i(\alpha + \sigma + \rho) + \omega)p_i \tag{A.13}$$

633 and

$$\frac{d\hat{p}_i}{dt}(t, ct + x_0) \geq -(\mu + f(t) + i(\alpha + \sigma + \rho) + \gamma + i\theta)\hat{p}_i(t, ct + x_0). \tag{A.14}$$

634 Using the Gronwall lemma once again, we obtain that for all $i \in \{0, \dots, I\}$,

$$p_i(t, x) \geq e^{-\int_0^t \mu + f(s) + i(\dots) + \omega ds} p_i(0, x) > 0 \tag{A.15}$$

635 and

$$\hat{p}_i(t, ct + x_0) \geq e^{-\int_0^t \mu + f(s) + i(\dots) + \gamma + i\theta ds} \hat{p}_i(0, x_0) > 0 \tag{A.16}$$

636 for all $t > 0$, $x \in \Omega$. This proves that as soon as the initial condition is positive, the solution

637 is positive for all $t > 0$. Then the total population of stationary hosts $N_I(t, x) := \sum_{i=0}^I p_i$

638 is positive, the total population of moving hosts $\hat{N}_I(t, x) := \sum_{i=0}^I \hat{p}_i$ is positive, the total

639 population of parasites in/on stationary hosts $P_I(t, x) := \sum_{i=0}^I i p_i$ is positive, and the total

640 population of parasites in/on moving hosts is $\hat{P}_I(t, x) := \sum_{i=0}^I i \hat{p}_i(t, x)$ is positive.

641 *Appendix A.4. System with N , m and A and their migratory counterpart*

642 Considering $N_I := \sum_{i=0}^I p_i$, $P_I := \sum_{i=0}^I i p_i$ and $Q_I = \sum_{i=0}^I i^2 p_i$ (see Appendix B for the
643 definition of Q), we obtain the following system of partial differential equations for N_I , P_I ,
644 Q_I and their moving counterparts (we omit the subscript I for N , P and Q and their moving
645 counterparts for simplicity of notation):

$$\left\{ \begin{array}{l}
 \frac{\partial N}{\partial t} = \beta(N + \hat{N}) - (\mu + \omega)N - \alpha P + \gamma \hat{N} + \theta \hat{P} \\
 \quad - \mathbf{p_I}(\lambda \mathbf{L} + \mathbf{p}) \\
 \frac{\partial P}{\partial t} = \lambda L N - (\mu + \omega + \sigma - \rho)P - \alpha Q + \gamma \hat{P} + \theta \hat{Q} \\
 \quad - \mathbf{p_I}(\lambda \mathbf{L}(\mathbf{1} + \mathbf{I}) + \rho(\mathbf{I}^2 + \mathbf{I})) \\
 \frac{\partial Q}{\partial t} = (\lambda L - \alpha g'''(1))N + (\sigma + 2\lambda L + 2\alpha + \rho)P \\
 \quad - (\mu + 2\sigma + \omega + 3\alpha - 2\rho) + \theta \hat{g}'''(1)\hat{N} - 2\theta \hat{P} + (\gamma + 3\theta)\hat{Q} \\
 \quad - \mathbf{p_I}(\lambda \mathbf{L}(\mathbf{I}^2 + \mathbf{2I} + \mathbf{1}) + \rho(\mathbf{I}^3 + \mathbf{2I} + \mathbf{I})) \\
 \frac{\partial \hat{N}}{\partial t} + c \frac{\partial \hat{N}}{\partial x} = \omega N - (\mu + \gamma)\hat{N} - (\alpha + \theta)\hat{P} \\
 \quad - \mathbf{p_I}(\dots) \\
 \frac{\partial \hat{P}}{\partial t} + c \frac{\partial \hat{P}}{\partial x} = \omega P + (\lambda L - (\alpha + \theta)\hat{g}'''(1))\hat{N} - (\mu + \sigma + \gamma - 2(\alpha + \theta) - \rho)\hat{P} - 3(\alpha + \theta)\hat{Q} \\
 \quad - \mathbf{p_I}(\dots) \\
 \frac{\partial \hat{Q}}{\partial t} + c \frac{\partial \hat{Q}}{\partial x} = \omega Q + (\lambda L - (\alpha + \theta)\hat{g}'''(1))\hat{N} + (\sigma + 2\lambda L + 2(\alpha + \theta) + \rho)\hat{P} \\
 \quad - (\mu + 2\sigma + \gamma + 3(\alpha + \theta) - 2\rho)\hat{Q} \\
 \quad - \mathbf{p_I}(\dots) \\
 \frac{\partial L}{\partial t} = \kappa(P + \hat{P}) - \mu_L L - \lambda L(N + \hat{N})
 \end{array} \right. \tag{A.17}$$

646 Because the sums are finite, we end up with some extra terms depending on I and p_I ,
647 highlighted in bold, which do not appear in the main problem (14 - 19). However, assuming

648 that for all $n \in \mathbb{N}$,

$$\lim_{I \rightarrow +\infty} \sum_{i=0}^I i^n p_i \text{ and } \lim_{I \rightarrow +\infty} \sum_{i=0}^I i^n \hat{p}_i \quad (\text{A.18})$$

649 exist for all $t > 0$, $x \in \Omega$, we can define $N_\infty := \lim_{I \rightarrow +\infty} N_I$, $P_\infty := \lim_{I \rightarrow +\infty} P_I$, $Q_\infty :=$
650 $\lim_{I \rightarrow +\infty} Q_I$, and their moving counterparts. This assumption roughly means that the dis-
651 tribution of parasites among hosts has finite moment, which is true, for instance, for the
652 Poisson or negative binomial distributions. This assumption was implicitly made (at least
653 up to $n = 3$) in Kretzschmar and Adler (1993). From this assumption we also obtain that
654 for I large enough and for all $n \in \mathbb{N}$,

$$p_I < I^{-n} \ll 1 \quad (\text{A.19})$$

655 and thus when I is large enough, system (A.17) can be approximated by

$$\left\{ \begin{array}{l} \frac{\partial N}{\partial t} = \beta(N + \hat{N}) - (\mu + \omega)N - \alpha P + \gamma \hat{N} + \theta \hat{P} \\ \frac{\partial P}{\partial t} = \lambda L N - (\mu + \omega + \sigma - \rho)P - \alpha Q + \gamma \hat{P} + \theta \hat{Q} \\ \frac{\partial Q}{\partial t} = (\lambda L - \alpha g'''(1))N + (\sigma + 2\lambda L + 2\alpha + \rho)P \\ \quad - (\mu + 2\sigma + \omega + 3\alpha - 2\rho) + \theta \hat{g}'''(1) \hat{N} - 2\theta \hat{P} + (\gamma + 3\theta) \hat{Q} \\ \frac{\partial \hat{N}}{\partial t} + c \frac{\partial \hat{N}}{\partial x} = \omega N - (\mu + \gamma) \hat{N} - (\alpha + \theta) \hat{P} \\ \frac{\partial \hat{P}}{\partial t} + c \frac{\partial \hat{P}}{\partial x} = \omega P + (\lambda L - (\alpha + \theta) \hat{g}'''(1)) \hat{N} - (\mu + \sigma + \gamma - 2(\alpha + \theta) - \rho) \hat{P} - 3(\alpha + \theta) \hat{Q} \\ \frac{\partial \hat{Q}}{\partial t} + c \frac{\partial \hat{Q}}{\partial x} = \omega Q + (\lambda L - (\alpha + \theta) \hat{g}'''(1)) \hat{N} + (\sigma + 2\lambda L + 2(\alpha + \theta) + \rho) \hat{P} \\ \quad - (\mu + 2\sigma + \gamma + 3(\alpha + \theta) - 2\rho) \hat{Q} \\ \frac{\partial L}{\partial t} = \kappa(P + \hat{P}) - \mu_L L - \lambda L(N + \hat{N}) \end{array} \right. \quad (\text{A.20})$$

656 which yields problem (14-19).

657 **Appendix B. Derivation of dynamic equations for the VMR**

658 Following the derivation of the non-spatial model of Kretzschmar and Adler (1993), we
 659 introduce a third aggregate variable, $Q = \sum i^2 p_i$ (and its migratory counterpart, \hat{Q}). The
 660 following equations describing the change in Q and \hat{Q} were found by multiplying equations
 661 (1-4) by i^2 and summing (as for P and \hat{P}):

$$\frac{\partial Q}{\partial t} = -(\mu + 2\sigma + \omega)Q + (\sigma + 2\phi)P + \phi N + \gamma\hat{Q} - \alpha N \sum_{i=0}^{\infty} i^3 r_i + \theta \hat{N} \sum_{i=0}^{\infty} i^3 \hat{r}_i \quad (\text{B.1})$$

$$\frac{\partial \hat{Q}}{\partial t} - c \frac{\partial \hat{Q}}{\partial x} = -(\mu + 2\sigma + \gamma)\hat{Q} + (\sigma + 2\phi)\hat{P} + \phi\hat{N} + \omega Q - (\alpha + \theta)\hat{N} \sum_{i=0}^{\infty} i^3 \hat{r}_i. \quad (\text{B.2})$$

662 Applying the chain rule as above, we can get equations for $u = Q/N$ and $\hat{u} = \hat{Q}/\hat{N}$. We
 663 can use a trick with probability generating functions to deal with the sums in equations
 664 (B.1-B.2). The sums can be expressed as:

$$\sum_{i=0}^{\infty} i^3 r_i = g'''(1) + 3u - 2m, \quad (\text{B.3})$$

665 where $g(z)$ is the probability generating function of the distribution of r_i (e.g., the negative
 666 binomial distribution), and $g'''(1)$ is the third derivative evaluated at $z = 1$ (see Appendix
 667 II of Kretzschmar and Adler (1993)). Inserting equation (B.3) into equations (B.1-B.2) and
 668 solving for $\partial u/\partial t$ and $\partial \hat{u}/\partial t - c \partial \hat{u}/\partial x$, we get

$$\frac{\partial u}{\partial t} = -u \left(2\sigma + \beta \left(\frac{N + \hat{N}}{N} \right) \right) + m(\sigma + 2\phi) + \phi - \alpha(g'''(1) + 3u - 2m - um) \quad (\text{B.4})$$

$$+ \frac{\hat{N}}{N} \left[\theta(\hat{g}'''(1) + 3\hat{u} - 2\hat{m} - \hat{m}u) + \gamma(\hat{u} - u) \right]$$

$$\begin{aligned} \frac{\partial \hat{u}}{\partial t} - c \frac{\partial \hat{u}}{\partial x} = & \hat{u} \left(\hat{m}(\alpha + \theta) - 2\sigma \right) + \hat{m}(\sigma + 2\phi) + \phi + \omega \frac{N}{\hat{N}}(u - \hat{u}) \\ & - (\alpha + \theta)(\hat{g}'''(1) + 3\hat{u} - 2\hat{m}) \end{aligned} \quad (\text{B.5})$$

669 The VMR, A , can be expressed in terms of u and m :

$$A = \frac{\text{variance}}{m} = \frac{\sum_{i=0}^{\infty} i^2 r_i - m^2}{m} = \frac{u - m^2}{m}. \quad (\text{B.6})$$

670 We can use equation (B.6) to obtain a differential equation for A of the form:

$$\frac{\partial A}{\partial t} = \frac{1}{m} \frac{\partial u}{\partial t} - \frac{u}{m^2} \frac{\partial m}{\partial t} - \frac{\partial m}{\partial t}. \quad (\text{B.7})$$

671 Using equations (B.1-B.2), (15), and (17), and substituting $u = m(A+m)$ and $\hat{u} = \hat{m}(\hat{A} + \hat{m})$,

672 we can write the equations for the change in the VMR:

$$\begin{aligned}
\frac{\partial A}{\partial t} = & \beta m \left(\frac{N + \hat{N}}{N} \right) - (A - 1) \left(\sigma + \frac{\phi}{m} \right) \\
& - \alpha \left(\frac{g'''(1)}{m} + 3(A + m) - (2 + m(A + m)) - A(A + 2m) \right) \\
& + \frac{\hat{N}}{Nm} \left[\theta \left(\hat{g}'''(1) + 3\hat{m}(\hat{A} + \hat{m}) - \hat{m}(2 + m(A + m)) - \hat{m}(\hat{A} + \hat{m} - m)(A + 2m) \right) \right. \\
& \left. + \gamma \left(\hat{m}(\hat{A} + \hat{m}) - m(A + m) - (A + 2m)(\hat{m} - m) \right) \right] \tag{B.8}
\end{aligned}$$

$$\begin{aligned}
\frac{\partial \hat{A}}{\partial t} - c \frac{\partial \hat{A}}{\partial x} = & (\alpha + \theta) \left[\hat{A}(3\hat{m} - 3 + \hat{A}) + \hat{m}(\hat{m} - 3) + 2 - \frac{\hat{g}'''(1)}{\hat{m}} \right] \\
& - (\hat{A} - 1) \left(\sigma + \frac{\phi}{\hat{m}} \right) + \omega \frac{Nm}{\hat{N}\hat{m}} \left(A + m + \frac{\hat{m}^2}{m} - \hat{A} - 2\hat{m} \right) \tag{B.9}
\end{aligned}$$

673 To apply the model in equations (14-17) and (B.8-B.9), we need to define $g'''(1)$ and
674 $\hat{g}'''(1)$ by assuming a distribution of parasites among hosts. Defining the distribution still
675 allows for the mean and VMR in the parasite burden to change in space and time, thus
676 accounting for changes in the overdispersion.

677 If we assume that parasites are distributed among hosts according to the negative bino-
678 mial, then we can make the substitutions:

$$\begin{aligned}
g'''(1) &= m(m + A - 1)(m + 2(A - 1)) \\
\hat{g}'''(1) &= \hat{m}(\hat{m} + \hat{A} - 1)(\hat{m} + 2(\hat{A} - 1)) \tag{B.10}
\end{aligned}$$

679 These substitutions simplify equations (B.8-B.9), yielding equations (18-19).

680 **Appendix C. Numerical methods**

681 We numerically simulated model solutions on a discrete space-time grid where:

$$x \rightarrow x_i \in \{x_0, x_1, \dots, x_{n_x}\}$$

$$t \rightarrow t_k \in \{t_0, t_1, \dots, t_{n_t}\}.$$

682 We set the grid spacing in the spatial domain, Δx , based on the length of the migration
683 route being considered such that n_x was reasonably large but still computationally feasible.

684 We then chose a sufficiently small time step that densities did not move more than one grid
685 space to avoid numerical errors (i.e., the Courant-Friedrichs-Lewy condition; Courant et al.,

686 1967). In general, the time step should be set to $\Delta t \approx \nu \Delta x / c$, where $0 \leq \nu \leq 1$ is the
687 Courant number and c is the migration speed. Note that if Δt is exactly $\Delta x / c$, then the

688 numerical approximation to the advection equation (step 1 below) is exact. This was the
689 case for our general simulations where we chose a migration speed of $c = 10000 \text{ km yr}^{-1}$

690 (Table 2), $\Delta x = 1 \text{ km}$, $\Delta t = 0.0001 \text{ yr}$, and $\nu = 1$. By using the exact solution, we avoided
691 the effect of “numerical diffusion”, whereby the numerical approximation of advection results

692 in a spreading out of the population densities. We denote the numerical approximation of
693 $\hat{N}(x_i, t_k)$ at point (i, k) on the grid as $\hat{N}_{i,k}$.

694 At each time step in the numerical simulation of the model, we split the model equations
695 into an advection processes, consisting of movement of migratory populations, and a reaction

696 process, consisting of temporal change in population densities, consisting of host birth/death,
697 parasite attachment/death, and switching status between migratory and stationary. As an

698 example, equation (16) can be written as:

$$\frac{\partial \hat{N}}{\partial t} = \underbrace{c \frac{\partial \hat{N}}{\partial x}}_A - \underbrace{\left(\mu + \gamma + (\alpha + \theta) \hat{m} \right) \hat{N} + \omega N}_{\mathcal{R}}$$

699 where \mathcal{A} is the advection process and \mathcal{R} is the reaction process.

700 We assumed Neumann boundary conditions where the derivative across the boundary
701 is zero. This was simulated by adding a ghost node onto either end of our spatial grid, at
702 $i = -1$ and $i = n_x + 1$. The numerical algorithm proceeded as follows. For each time step k
703 in 1 to n_t :

- 704 1. Force boundary conditions by setting $\hat{N}_{-1,k} = \hat{N}_{1,k}$ and $\hat{N}_{n_x+1,k} = \hat{N}_{n_x-1,k}$.
- 705 2. Solve $\frac{\partial \hat{N}_{\mathcal{A}}}{\partial t} = \mathcal{A}$ with $\hat{N}_{\mathcal{A}}(x_i, 0) = \hat{N}_{i,k}$ on $[0, \Delta t]$ using a finite upstream differencing
706 method (Hundsdoerfer and Verwer, 2013).
- 707 3. Solve $\frac{\partial \hat{N}_{\mathcal{R}}}{\partial t} = \mathcal{R}$ with $\hat{N}_{\mathcal{R}}(x_i, 0) = \hat{N}_{\mathcal{A}}(x_i, \Delta t)$ on $[0, \Delta t]$ using a fourth-order Runge-
708 Kutta method.
- 709 4. Set $\hat{N}_{i,k+1} = \hat{N}_{\mathcal{R}}(x_i, \Delta t)$.

710 The above scheme is written for \hat{N} , but at each step, the algorithm was applied to the other
711 variables as well. Note, however, that for the non-migratory variables N , m , A , and L ,
712 $\mathcal{A} = 0$ and thus $N_{\mathcal{A}}(x_i, \Delta t) = N_{i,k}$.